



Numerical and experimental investigation on material flow in gear forced throughfeed rolling process

Ziyong Ma¹ · Yuanxin Luo^{1,2,3} · Yongqin Wang^{1,2} · Dave C. Willens⁴

Received: 10 August 2018 / Accepted: 20 May 2019 / Published online: 21 June 2019
© Springer-Verlag London Ltd., part of Springer Nature 2019

Abstract

The cylindrical die forced throughfeed rolling process for gears was proposed to overcome an end-effect behavior of the standard radial-feed gear rolling process which can result in pitch variation and excessive axial end-flow. In the rolling process, the workpieces are pushed through the gap of the rolling tools to form the gear teeth. Understanding of material flow is important for grasping the cause of defect formation and improving the quality of formed gears. In this paper, the material flow behavior of the gear forced throughfeed rolling process was studied on the flow velocity and displacement of key locations by using finite element analysis (FEA). The experiment was also conducted and its blank was sliced to thin pieces, and the grid pattern (GP) was utilized to track the trajectory of flowing materials. The results show that the end-flow is located at the root rather than the tooth crest of the formed workpiece, because the compressive forces from rolling tool mainly take effect at the root of the formed workpiece. The asymmetry of circumferential flow displacements with respect to the gear teeth results in the asymmetrical flanks defect, and this is due to the meshing between teeth of rolling tool and workpiece. The local displacement in the radial direction is larger than that in the circumferential direction.

Keywords Gear forced throughfeed rolling process · Material flow · FEA · Grid pattern (GP)

1 Introduction

The roll forming process, commonly used in the manufacture of precision splines and helical screw threads, is an innovative metal forming technology having the advantages of material savings, high production efficiency, and improved mechanical fatigue properties. For these reasons, this process has great potential for manufacturing multi-tooth cylindrical gear forms for torque transmission applications, and it has been studied extensively in recent years. Kamouneh et al. [1, 2] analyzed

three forming defects in the rolling process, some possible solutions for controlling the defects, and the impact of the forming process on tooth strength by using the finite element analysis (FEA). Neugebauer et al. [3–5] discussed flat die and cylindrical die gear rolling techniques and proposed a variable-pitch forming die design with synchronized workpiece driving to improve gear teeth quality. Khodae and Melander [6] explored the shape accuracy of roll-formed gears with module 1 mm and 4 mm using DEFORM® simulation software. Kretzschmar et al. [7] measured the forming loads and stresses at the die to workpiece contact zone in the rolling process by a test platform, and the contact stress of the tool surface is calculated by a simulation package. Li et al. [8, 9] studied the factors that affect slippage in the teeth-dividing stage based on numerical simulation and experiment, and the cause of rabbit ear formation due to the friction force was also analyzed. Ma et al. [10, 11] investigated the root cause of pitch error induced during the initial stage of the gear throughfeed rolling process and the effects of other relevant factors on pitch error by theoretical models, FEA, and experiments. Zhu et al. [12] verified the feasibility of the hot roll forming process for large module spur gear manufacturing by also using FEA and experiment.

✉ Yuanxin Luo
yxluo@cqu.edu.cn

¹ College of Mechanical Engineering, Chongqing University, Chongqing 400044, China

² State Key Lab of Mechanical Transmission, Chongqing University, Chongqing 400044, China

³ National Demonstration Center for Experimental Mechanical Foundation Education, Chongqing University, Chongqing 400044, China

⁴ Kinefac Corporation, Worcester, MA 01603, USA

One of the intrinsic characteristics of the gear roll forming process is that the material flow velocity gradient over the gear cross section varies because the workpiece material is in direct contact with the tooth surface of rolling tool. The flow velocity of material closed to the interface is faster than the other region due to the friction at the forming interface. The inhomogeneity of material flow velocity has a direct effect on the quality of the formed tooth top. Recent research work pertaining to the metal flow in the roll forming process mainly focuses on the forming of splines and helical threads. Domblesky and Feng [13] examined the effect of rolling parameters on material flow and profile geometry in external thread rolling of large diameter blanks based on numerical results. Sieczkarek et al. [14] analyzed the difference between incipient and repeatable metal flow in the incremental sheet-bulk forming of gears through FEA and experiment. Yan et al. [15] investigated the effect of the thread helix angle on metal flow from the perspective of rolling force using DEFORM®, and the results demonstrate that the metal flow velocity increases as the helix angle of rolling dies increases. Cui et al. [16] investigated the metal flow in involute splines formed by the cold roll-beating process by using theoretical analysis, FEA, and experiment. The results show that the material flow directions are determined by the minimum moving resistance. Liu et al. [17] analyzed the influence of involute spline rolling process parameters on rolling force and spindle torque by installing a force measuring system. The workpiece hardness and wear resistance were also obtained.

The finite element method is suitable for predicting various characteristics of the roll forming process, including the material flow behavior, forming stresses, strains, and the temperature of each stage during rolling. This information is helpful to the understanding of the process and forming mechanisms leading to process-related defects. Therefore, numerical simulation is a very powerful method in studying the material flow of metal forming at present. Pater et al. [18] demonstrated the feasibility of a new thread rolling method using FEA and experiments performed in laboratory conditions and industrial tests. Szota and Dyja [19] presented a computer simulation of the rolling of round reinforcement bar and determined the metal flow behavior as well as the effects of roller shape and dimensions on the pitch of the finished bar. Groche and Kramer [20] simulated the rolling process with flat dies and consideration of friction and analyzed the tribological characteristics and friction effect based on FEA. Zhang and Zhao [21] developed a new rolling process for a shaft with a thread and spline which is based on two-die cross rolling technology. The virtual forming behaviors of the new rolling process were simulated by FEA. Cui et al. [22] introduced an axial-push incremental warm rolling process for a spline shaft of 42CrMo material and analyzed its formation mechanism, die angle optimization, and process parameter selection by using FEA. However, very few

research efforts have been made on the material flow of the gear forced throughfeed rolling process.

An in-deep understanding of the material flow behavior in the gear throughfeed rolling process is beneficial to the optimization of processing parameters and the identification of the forming cause to some defects. Therefore, this work aims to investigate the material flow behavior in the gear forced throughfeed rolling process by using FEA and physical experiments. The rest of the paper is organized as follows: Section 2 describes the working principles of the gear forced throughfeed rolling process, Section 3 presents the finite element modeling and analysis results of the gear throughfeed rolling process, Section 4 gives the experimental results, Section 5 presents the influence of metal flow on resulting microstructure, and finally, some conclusions are given in Section 6.

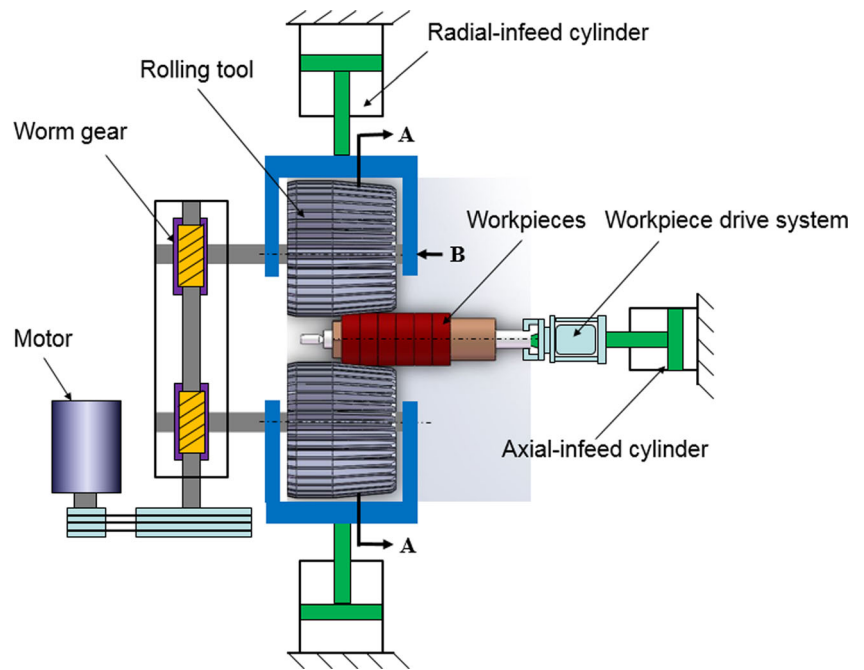
2 Principles of the gear throughfeed rolling process

2.1 Gear throughfeed rolling process

The cylindrical die forced throughfeed rolling process for gears was proposed to overcome the end-effect behavior of the standard radial infeed gear rolling process which can result in pitch variation and excessive axial end-flow. The schematic diagram of the forced throughfeed rolling process for the present study is shown in Fig. 1. A workpiece or a number of workpieces (shown in red color) are mounted to a rotating workpiece drive system which is fixed to and driven by an axial feed cylinder located on the machine rolling centerline. Two cylindrical rolling dies with the gear form on their periphery are positioned on either side of the workpiece parallel to the workpiece rolling centerline axis. The rolling dies are driven rotationally by a dual-output worm gearbox which is powered by an electric motor. The rotating speed of two rolling tools can be changed by varying the applied voltage to the motor. Note that a servo motor is adopted to keep a constant speed ratio between the workpiece and rolling tools. The gap between two rolling tools is adjusted by two radial-feed cylinders [23].

The working principle of the process can be divided into five steps: (1) the hollow workpieces are strung together by a mandrel which is fixed to the workpiece drive system; (2) the rolling tools are actuated by the radial infeed cylinders until the desired gap is achieved; (3) the rolling tools and workpieces are rotated by the motor and workpiece drive system, respectively, according to the matching gear ratio; (4) the workpieces are pushed axially through the gap between the rotating forming dies by the axial feed cylinder; and (5) the desired gear tooth profile geometry is progressively formed into the workpiece as it passes through the forming dies.

Fig. 1 Working principle of the gear forced throughfeed rolling process [24]



2.2 Rolling tool

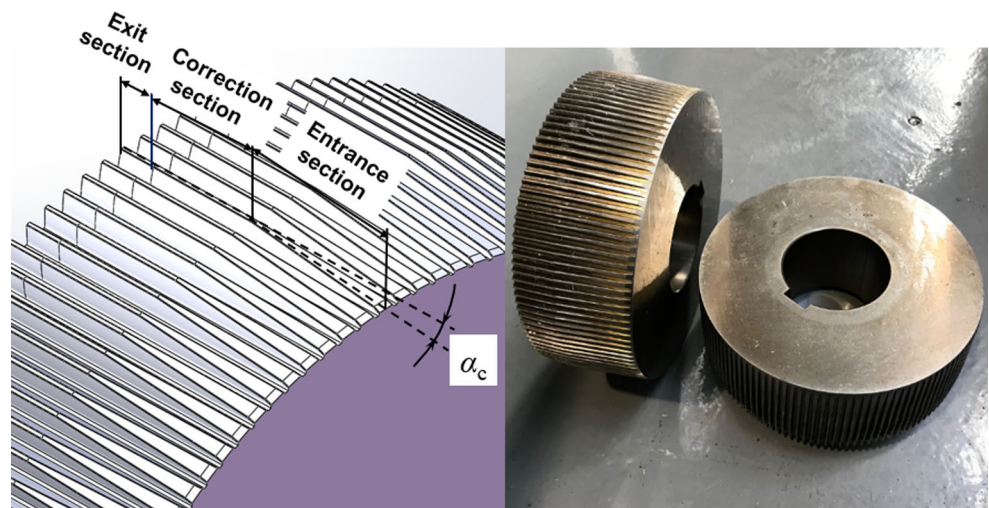
The cylindrical rolling tools (dies) are one of the key components of the gear rolling process. Manufacturing accuracy and mechanical properties of the tools have a significant impact on the quality of formed products. The die form geometry will affect the metal flow behavior. In this study, the forced throughfeed rolling tools are divided into three sections: the entrance section, correction section, and exit section according to the characteristic of the gear throughfeed rolling process [24], as shown in Fig. 2.

1. Entrance section: The entrance section is the main forming area of the workpiece and tool. The cone angle (α_c) is the key geometric parameter in this section because

it not only directly affects the metal flow of the workpiece but also has a great effect on the proportion of the radial force, axial force, and circumferential force component in the roll forming process.

2. Correction section: The correction section calibrates the final rolled form and does so over a certain number of workpiece revolutions controlled by the axial feed rate. The tooth profile accuracy and length of the correction section are the key geometric parameters because these characteristics determine the final quality of the rolled profile accuracy. Larger tooth depths can weaken the load carrying capacity of the individual die teeth, whereas shallower tooth depths can result in a sharp increase of die root stress due to the metal filling the entire tooth space.

Fig. 2 Structure design of rolling tool



- Exit section: The exit section gradually relieves the rolling stresses off the dies and workpiece to prevent damage to the workpiece surface and die teeth as the workpiece passes through. The die tooth profile in the exit section is designed as negative addendum modification and also serves to compensate for any elastic deflection of the rolling machine components as the rolling forces fluctuate.

3 Finite element simulation

3.1 Finite element modeling

FEA software allows detailed observations of the metal flow inside and on the surface of the workpiece subjected to metal forming. Meanwhile, there is no report on a perfect experimental method for quantifying the three-dimensional deformation and flow characteristics of metal in the open literature so far. Therefore, FEA is still the prevailing method to evaluate the three-dimensional flow behavior in metal forming processes. In this study, DEFORM-3D® by Scientific Forming Technologies Corporation in Columbus, Ohio, was utilized to simulate the roll forming process in the large deformation simulation. All simulations were run on a computer workstation with a CPU of Intel Xeon E5-2670 v2 and 128 GB RAM.

Due to the symmetry and forming similarity of each tooth, a 1/23 model with a thickness of 15 mm was established and constrained by two plates. The model was imported into the FEA preprocessor, as shown in Fig. 3.

3.2 Simulation conditions

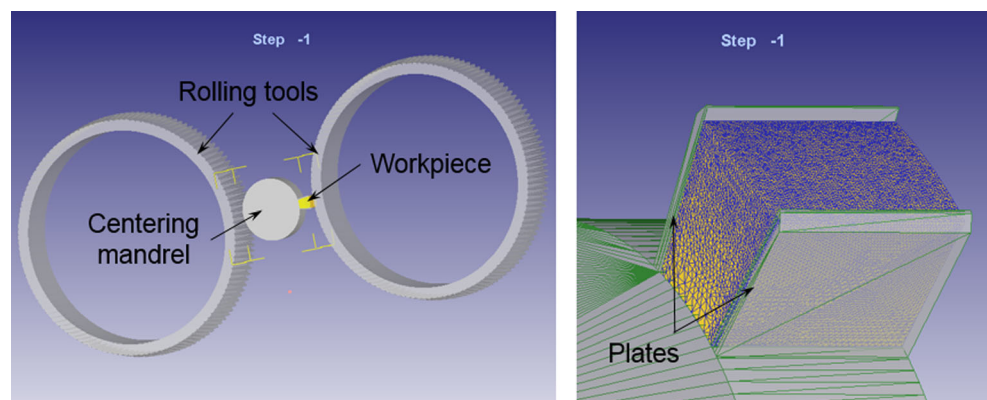
To make the FEA consistent with the practical situation, the simulation conditions were set correctly to ensure the accuracy, besides the geometry of the FEA model. The detailed parameter settings were as follows:

- Material properties: The workpiece whose initial size was $\Phi 80.66 \text{ mm} \times 15 \text{ mm}$ (diameter \times thickness) was set as a plastic body, and its material was defined as Al6061 corresponding to the material in the library AL-6061-T6, cold. The rolling tools were set as a rigid body, and the environment temperature was set at 20 °C.
- Grid parameters: Tetrahedral element type and relative mesh mode were selected in all simulations. The number of elements was about 150,000, and the minimum element size was approximated to 0.12 mm. A ring region was selected with the thickness of 5 mm and a density ratio of 0.01.
- Motion parameters: The rolling tools were set to rotate at a speed of 30 rpm and revolved at 83.48 rpm around the axis of the centering mandrel, and the axial feeding speed of the rolling tools was set at 0.7 mm/s.
- Friction parameter: Constant shearing friction was selected, and the friction coefficient on the contact zone of the rolling tools and workpiece was set at 0.3 [25, 26]. The workpiece was fixed to the centering mandrel, and other friction coefficient was set at 0.
- Simulation control: The total stroke of the rolling tools was set as 53 mm, and the number of simulation steps was set at 2000. The time step increment was 0.04 s/step, and the relative interference depth was set as 0.1 mm.

3.3 Simulation results

Previous research [27–30] estimated the material flow of incremental bulk forming processes by analyzing the stress, the strain rate, and the strain distribution at different positions of the workpiece at different forming stages. To characterize the material flow of the workpiece subjected to the rolling load, axial metal flow and radial metal flow as well as circumferential metal flow were determined by the point-tracking option in DEFORM®. It should be noted that the displacement of several material particles was recorded after the rolling process, whereas the flow velocity of different points was

Fig. 3 FEA model [24]



collected during the rolling process. To better understand the material flow along different directions during the rolling process, several points on the different planes of the rolled workpiece were tracked, and their positions are shown in Fig. 4.

3.3.1 Axial material flow behavior

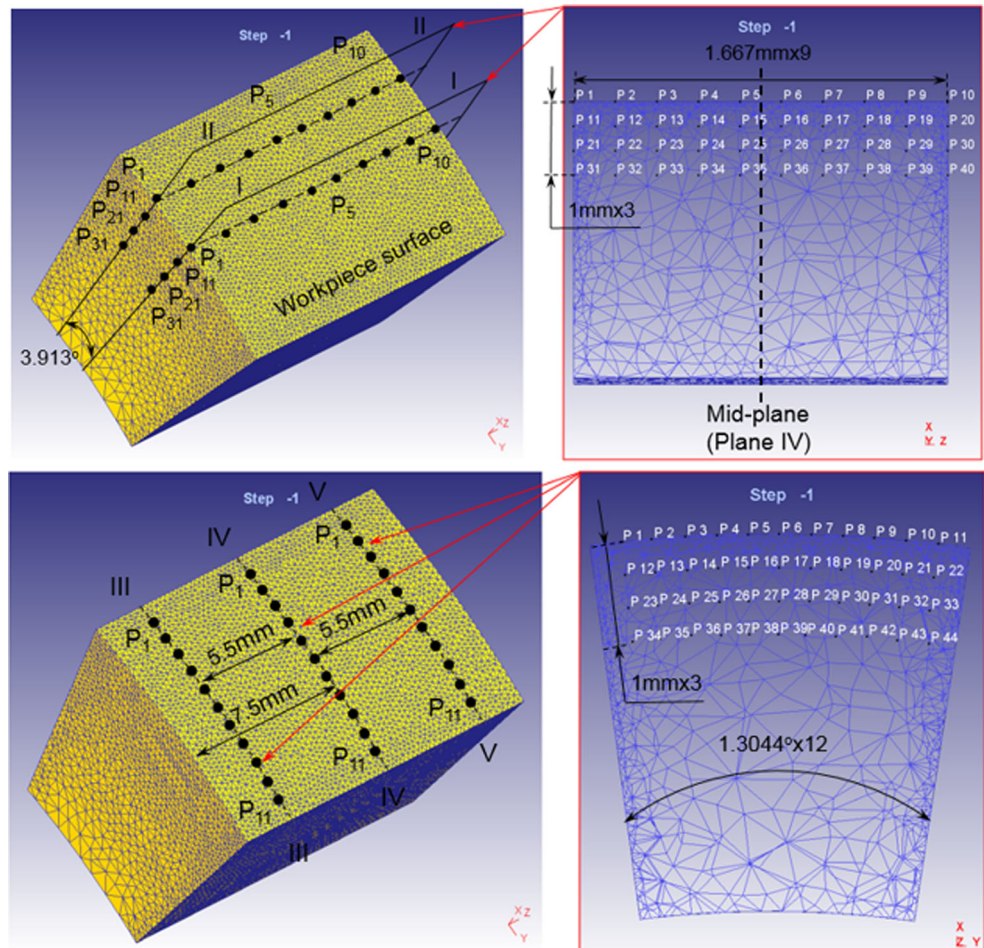
Axial flow velocity Figure 5 a shows the axial flow velocities of different points ($P_1 \sim P_{40}$) on plane I of the formed workpiece. It can be seen that the axial velocity changes of points at the depths of 0 mm, 1 mm, 2 mm, and 3 mm are similar except for the changes at $t = 13.31$ s. Here, the depth is the distance between analysis points and workpiece surface and the flow velocities of the points $P_1 \sim P_4$ and $P_7 \sim P_{10}$ on the workpiece surface first increase and then decrease with time. The axial velocities of the points $P_1, P_{11}, P_{21},$ and P_{31} and of the points $P_{10}, P_{20}, P_{30},$ and P_{40} at the depths of 0 mm, 1 mm, 2 mm, and 3 mm are the largest during the rolling process. However, the velocities of the points $P_5, P_6, P_{15}, P_{16}, P_{25}, P_{26}, P_{35},$ and P_{36} near the mid-plane (plane IV) at the depths of 0 mm, 1 mm, 2 mm, and 3 mm are relatively smaller, and there is no distinct pattern of variation during the forming stage. The reason for the variation is that the material particles near the workpiece

end-flow with less resistance than particles near the mid-plane (plane IV) due to the axial support of surrounding material. Additionally, it is also observed that the velocities of all points become zero in the finishing stage.

As can be seen from Fig. 5 b, the time interval between the axial velocities of P_1 to P_5 and P_6 to P_{10} on plane II of the formed workpiece is due to the time order of the contact between the rolling tool and workpiece, and the greater the depth, the smaller the flow velocity becomes. Additionally, the axial velocities of P_5 and P_7 are also observed to have a sudden change in the forming stage and finishing stage. This is because the teeth of rolling tools are in direct contact with the workpiece material very near these two points. Furthermore, the axial material flow on plane II of the formed workpiece is faster than the flow on plane I of the formed workpiece, which indicates the axial end-flow of rolled material is located near plane II and not near plane I of the formed workpiece, as shown in Fig. 5 c.

From Fig. 5 a and b, it can be observed that there is a neutral plane between the points $P_3, P_{13}, P_{23},$ and P_{33} and points $P_6, P_{16}, P_{26},$ and P_{36} , where the material neither flows forward nor flows behind in the axial direction. This is also identified by the axial velocity vector diagram, as shown in

Fig. 4 Position of moving points



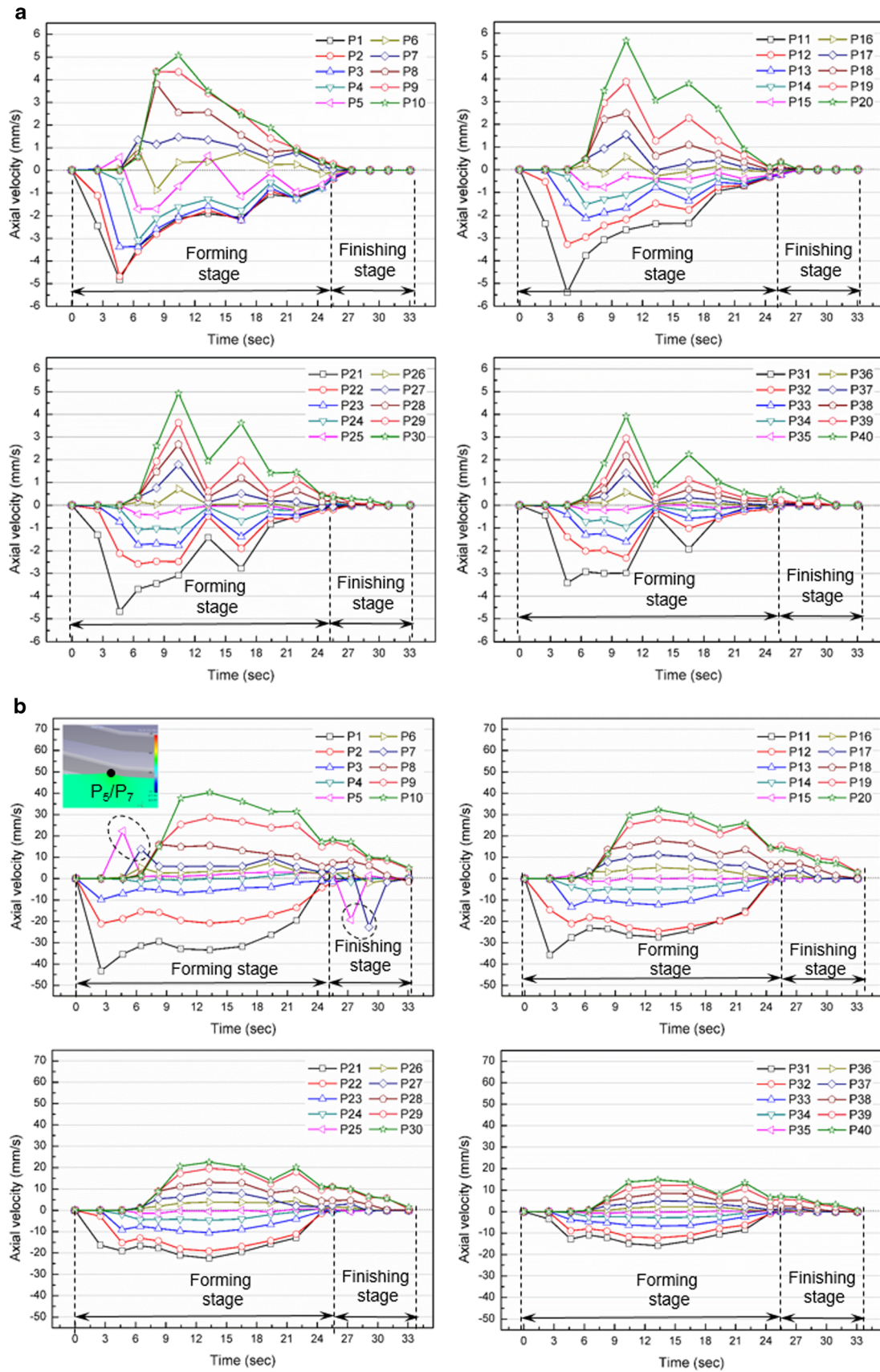


Fig. 5 Axial velocities of points on different planes. **a** Axial velocities of points on plane I of the formed workpiece. **b** Axial velocities of points on plane II of the formed workpiece. **c** End-flow morphology of the formed workpiece. **d** Neutral plane of axial flow velocity

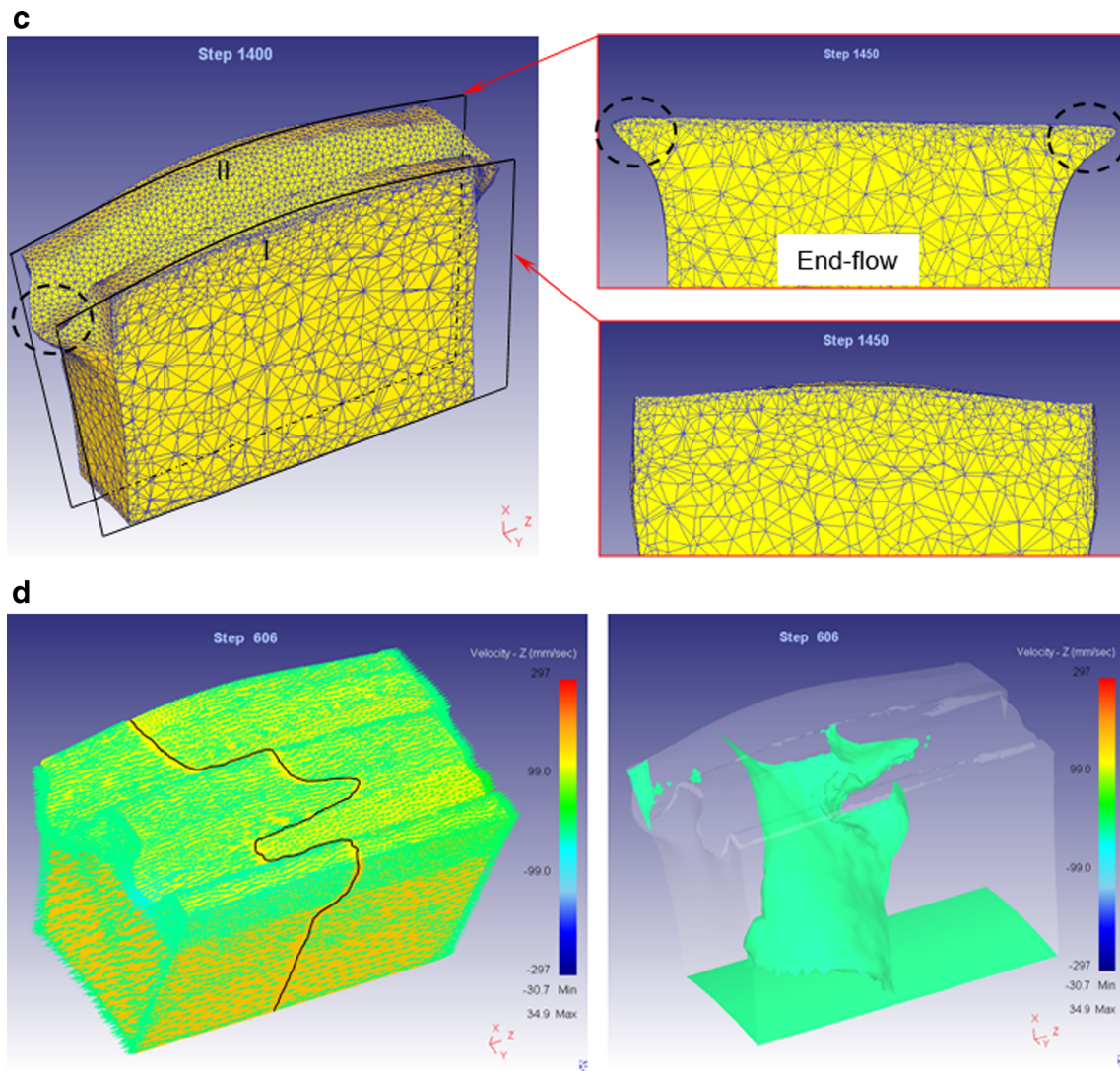


Fig. 5 (continued)

Fig. 5 d. It can be seen that the neutral plane is not a curved surface of sphere and its shape changes with time, which causes the material between the points $P_3, P_{13}, P_{23},$ and P_{33} and points $P_6, P_{16}, P_{26},$ and P_{36} at the depths of 0 mm, 1 mm, 2 mm, and 3 mm to hardly flow in the axial direction.

Axial displacement Flow velocity describes the magnitude and direction of material flow at different time intervals while the displacement describes the cumulative effects of material flow. The magnitude of displacement is also a result of the flow velocity. The axial displacements of different points are depicted in Fig. 6.

It can be seen from Fig. 6 a that the maximum axial displacements of material particles on plane I first increase and then decrease with the increase of depths. However, the maximum axial displacements of material particles on plane II

keep falling with depths, as shown in Fig. 6 b. The forward axial flow displacements and backward axial end-flow displacements of material particles on planes I and II are different during the rolling process.

By comparing the simulation results from Fig. 6 a and b, it is observed that the axial displacement trends at the tooth crest and root (the depth is 0 mm) of the formed workpiece are similar. However, the average axial displacement of P_1 and P_{10} at the tooth crest amounts to about 15.4% of that at the root, which indicates that the end-flow appears at the root rather than the tooth crest of the formed workpiece. The axial displacement at the tooth crest is almost symmetrical about the mid-plane (plane IV) but asymmetrical at the root. The reason for this behavior is believed to be the difference in frictional resistance to material flow between the tool tooth crest and the formed workpiece root.

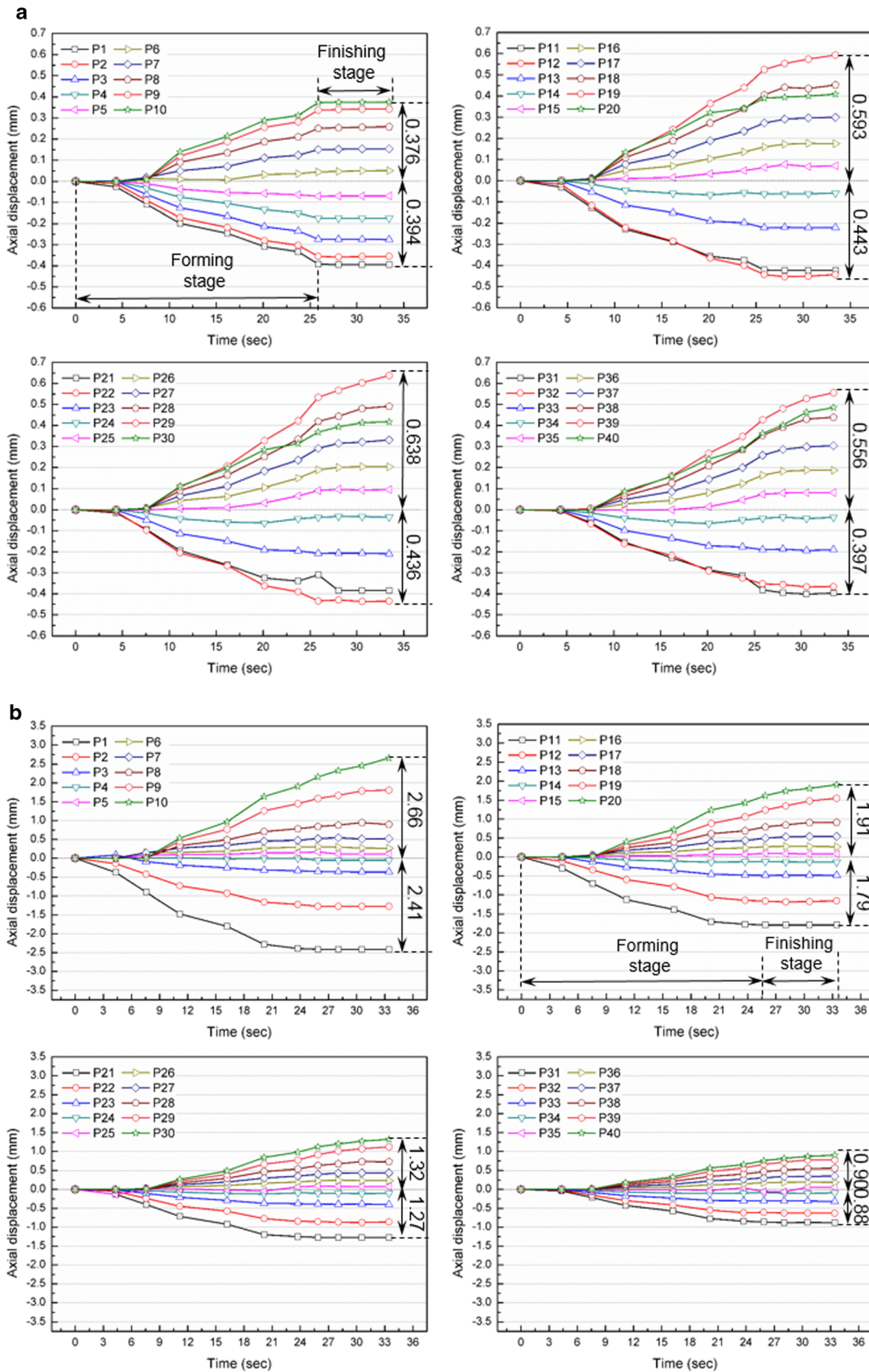


Fig. 6 Axial displacements of points at different planes. **a** Axial displacements of points on plane I of the formed workpiece. **b** Axial displacements of points on plane II of the formed workpiece

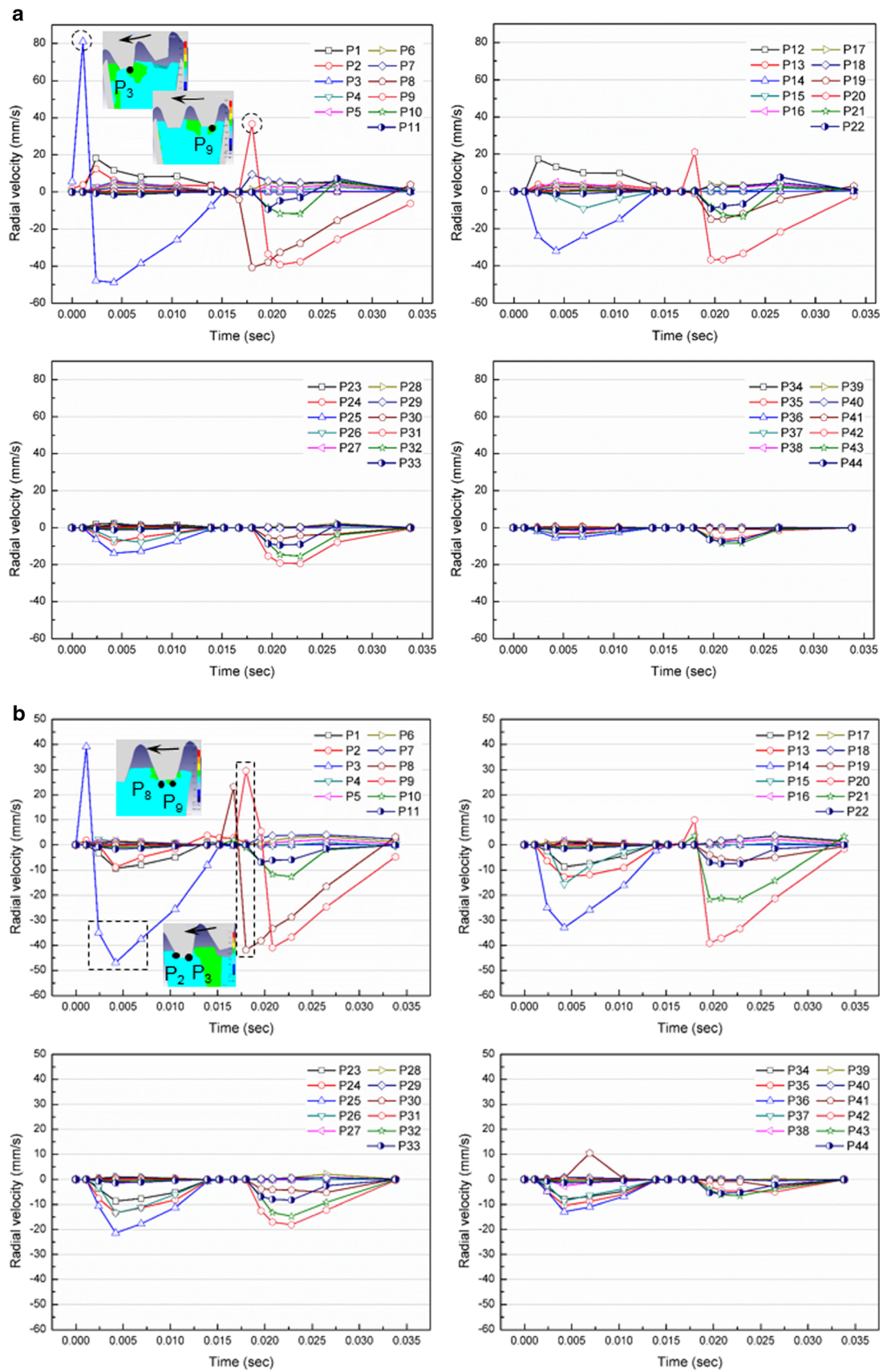


Fig. 7 Radial velocities of points at different planes. **a** Radial velocities of points on plane IV. **b** Radial velocities of points on plane III. **c** Radial velocities of points on plane V

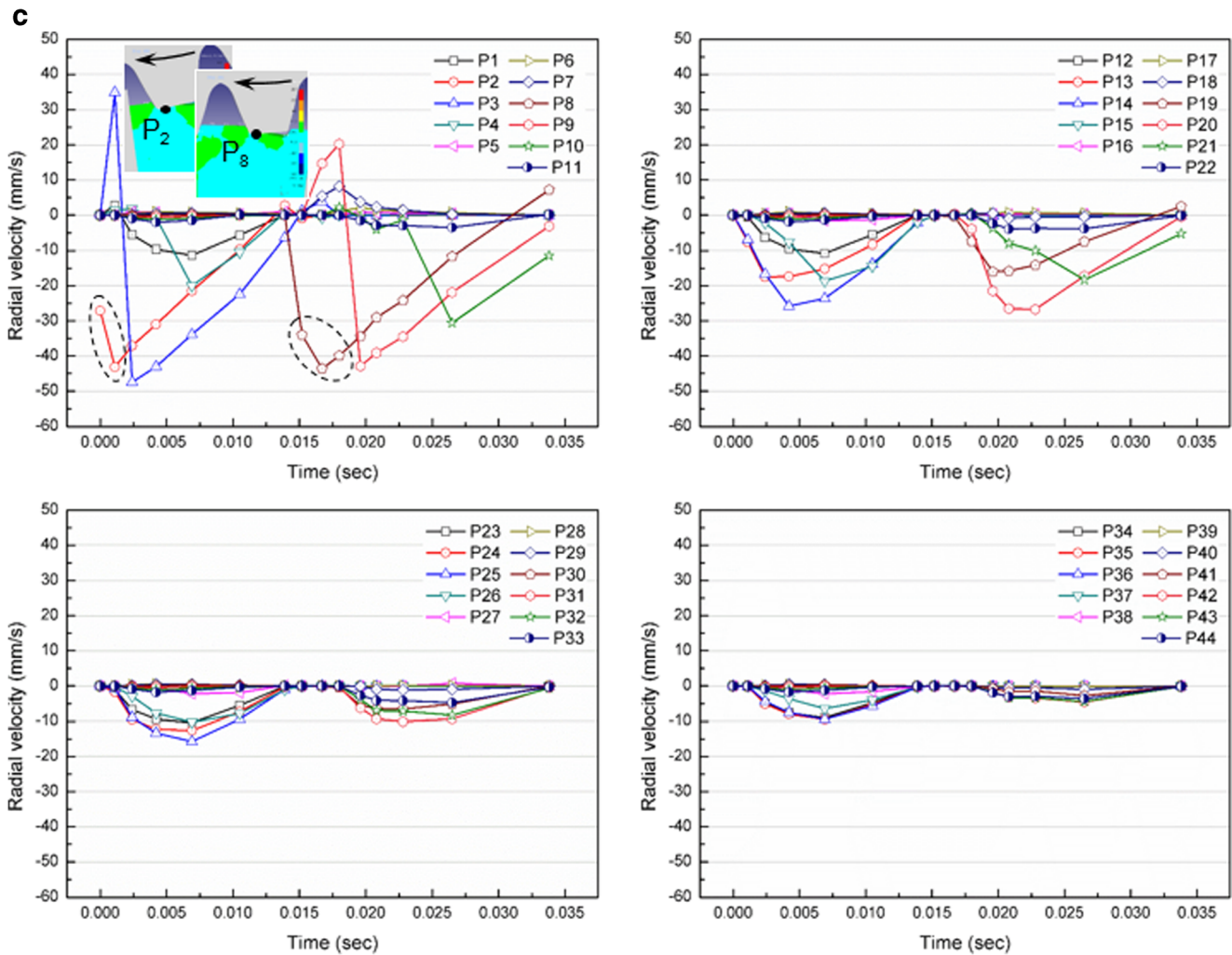


Fig. 7 (continued)

3.3.2 Radial material flow behavior

As mentioned in Section 3.3.1, the material near the mid-plane (plane IV) hardly flows in the axial direction during the gear rolling process. To clearly understand the material flow behavior in the radial direction, the radial flow velocity and displacement of points on different planes of an individual formed tooth were studied, as shown in Figs. 7 and 8.

Radial flow velocity Figure 7 displays the radial velocities of points on planes III, IV, and V in a time interval. It can be seen from Fig. 7 a that besides the significant velocity fluctuations in P_3 , P_8 , P_9 , P_{14} , and P_{20} on plane IV, the velocities of other points vary slowly in the range of -20 mm/s to 20 mm/s. The reason for this behavior is that these points reside in the root of the rolled form and are mainly subject to radial compressive forces from the forming tool toward the centerline axis of the workpiece. Additionally, the greater the depth, the smaller the radial velocity becomes.

It is also found from Fig. 7 b and c that the radial velocity trends of points on planes III and V are similar but not exactly the same, and that the velocity of P_2 at the range of $t = 0$ s to $t = 0.0125$ s in a given period is significantly different. This behavior is explainable because the tool tooth crest width on plane V is larger than the tool tooth crest width on plane III and because P_2 on plane V is located at the root whereas P_2 on plane III has moved to the tooth flank.

Radial displacement From Fig. 8 a, it is observed that the maximum radial displacement of material particles at the tooth crest and root of the formed workpiece is about 1 mm and -2 mm, respectively. However, the radial displacements of most material particles at the depths of 1 mm, 2 mm, and 3 mm are negative, which indicates that the material particles mainly flow toward the workpiece center due to the radial compressive forces from the rolling tool. Moreover, the radial displacements of material particles at different depths become increasingly smaller due to the increasing depth.

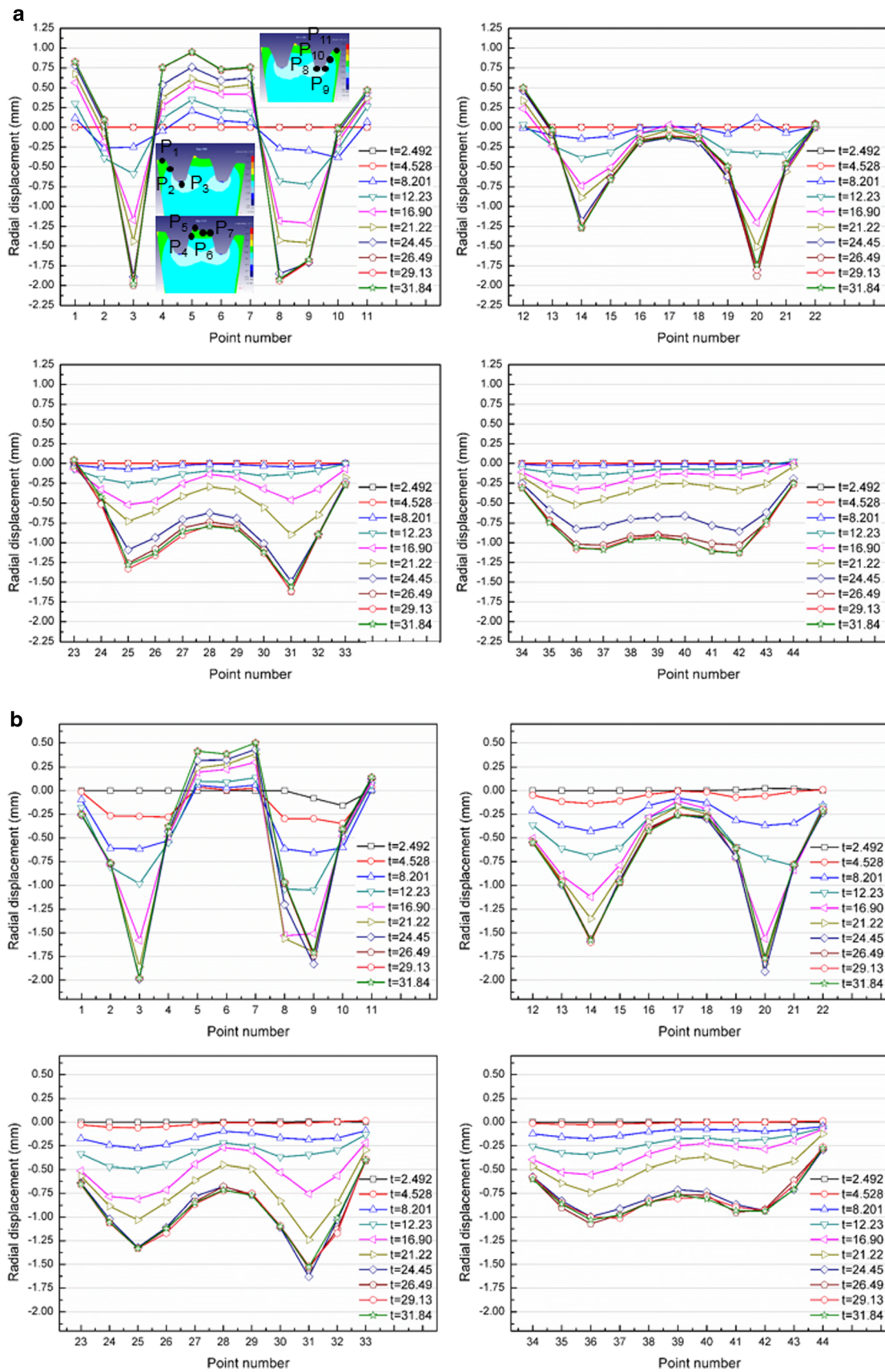


Fig. 8 Radial displacements of points at different planes. **a** Radial displacements of points on plane IV. **b** Radial displacements of points on plane III. **c** Radial displacements of points on plane V

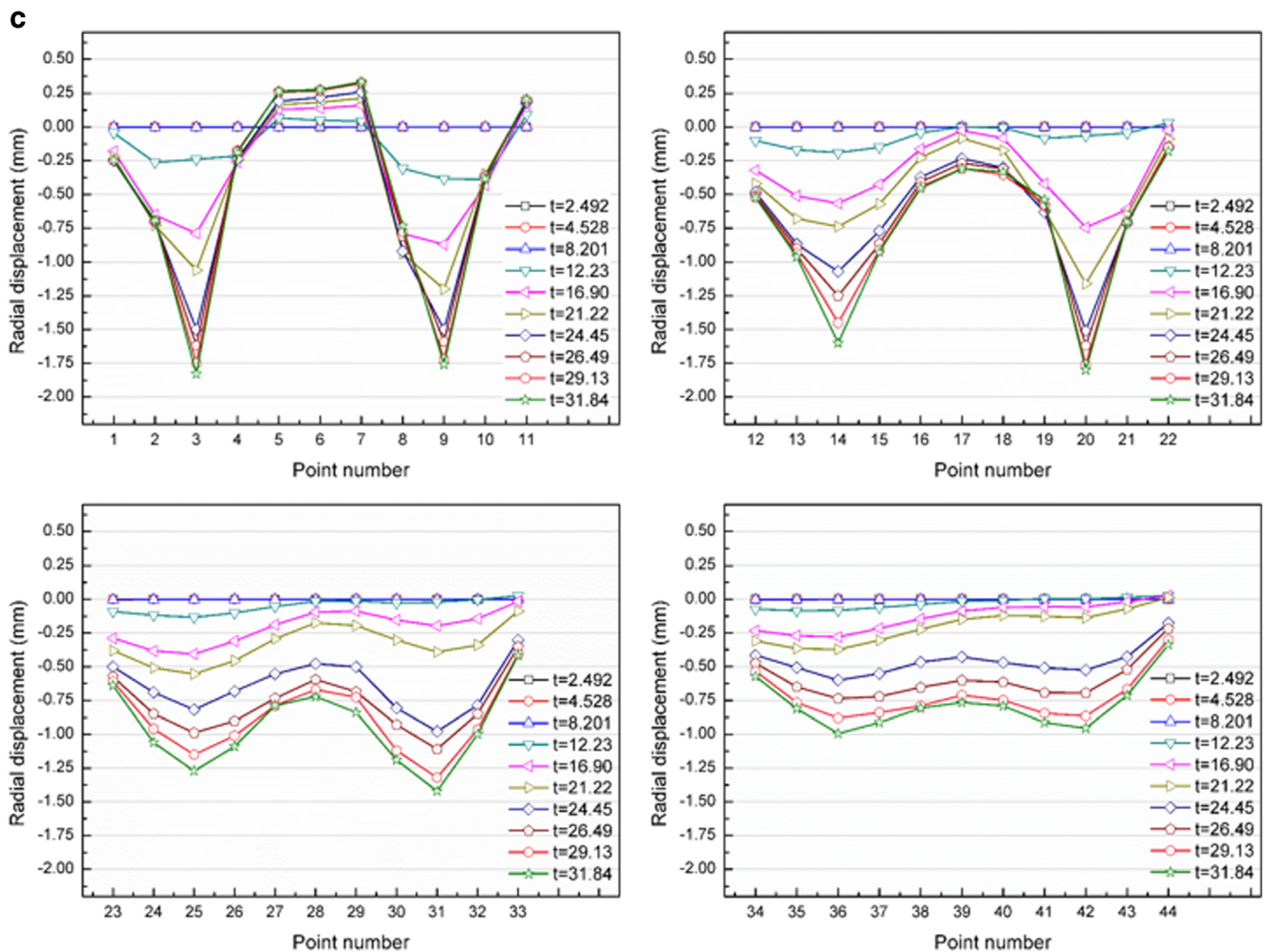


Fig. 8 (continued)

By observing the simulation results in Fig. 8 b and c, it is found that the radial displacements of material particles on planes III and V are very similar, and that the radial displacements of material particles at the formed crest and root increase as the rolling time increases, with the larger displacement occurring at the tooth root. Compared to the radial displacements of material particles at the tooth crest on plane IV, the radial displacement at the tooth crests on planes III and V is reduced by 47.3% and 64.5%, respectively. This indicates that the material on planes III and V mainly flows in the axial direction due to the absence of surrounding supporting material to resist the flow. Additionally, the radial displacement differences of material particles at the formed crests result in the rabbit ear formation due to the velocity gradient of material particles at the tooth crests.

3.3.3 Circumferential material flow behavior

Circumferential flow velocity The circumferential material flow behavior on the flanks of the workpiece is due to the sweeping effect from the tooth geometry of the rolling tools,

and it has a significant impact on the quality of formed workpieces. This is due to the fact that the asymmetry of circumferential material flow will result in the asymmetrical flanks of formed teeth. The circumferential flow velocity and displacement on different planes of the workpiece in a time period can be seen in Figs. 9 and 10.

It can be observed from Fig. 9 a that the circumferential flow velocity trend of material particles at the different depths on plane IV is similar and the velocity values decrease as the depth increases within a given time period. Moreover, the circumferential velocity values of most material particles are found to be positive in the given time interval, which indicates that the material mainly flows in the positive circumferential direction but not in the negative circumferential direction. Additionally, the circumferential flow velocities of material particles near P_3 , P_8 , and P_9 have significant fluctuation. This can be explained because these three points are located at the root of the formed workpiece.

By comparing the results in Fig. 9 b and c, it is found that circumferential velocity changes of material particles on planes III and V are very similar. However, there exist

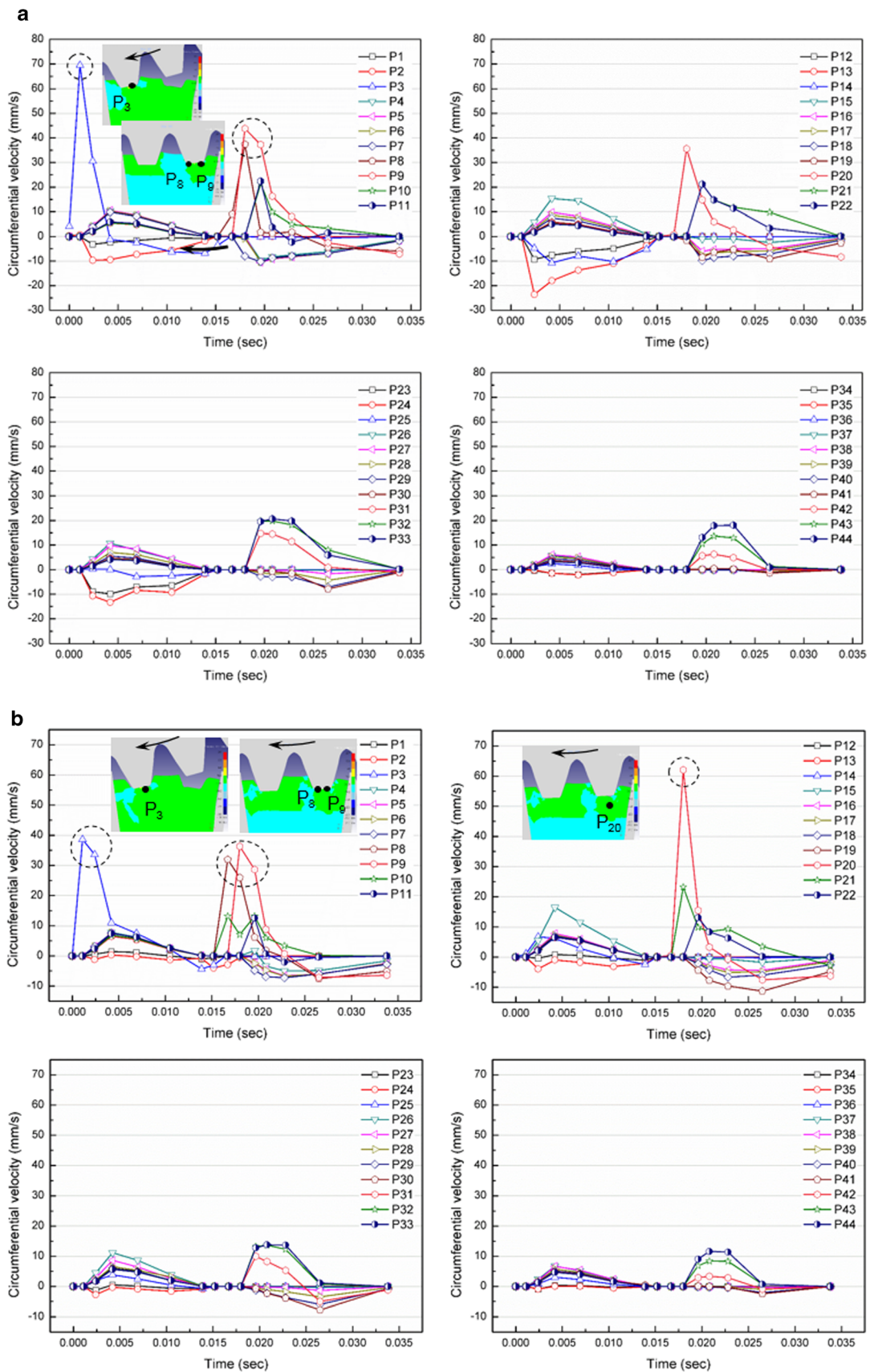


Fig. 9 Circumferential velocity of points at different planes. **a** Circumferential velocity of points on plane IV. **b** Circumferential velocity of points on plane III. **c** Circumferential velocity of points on plane V

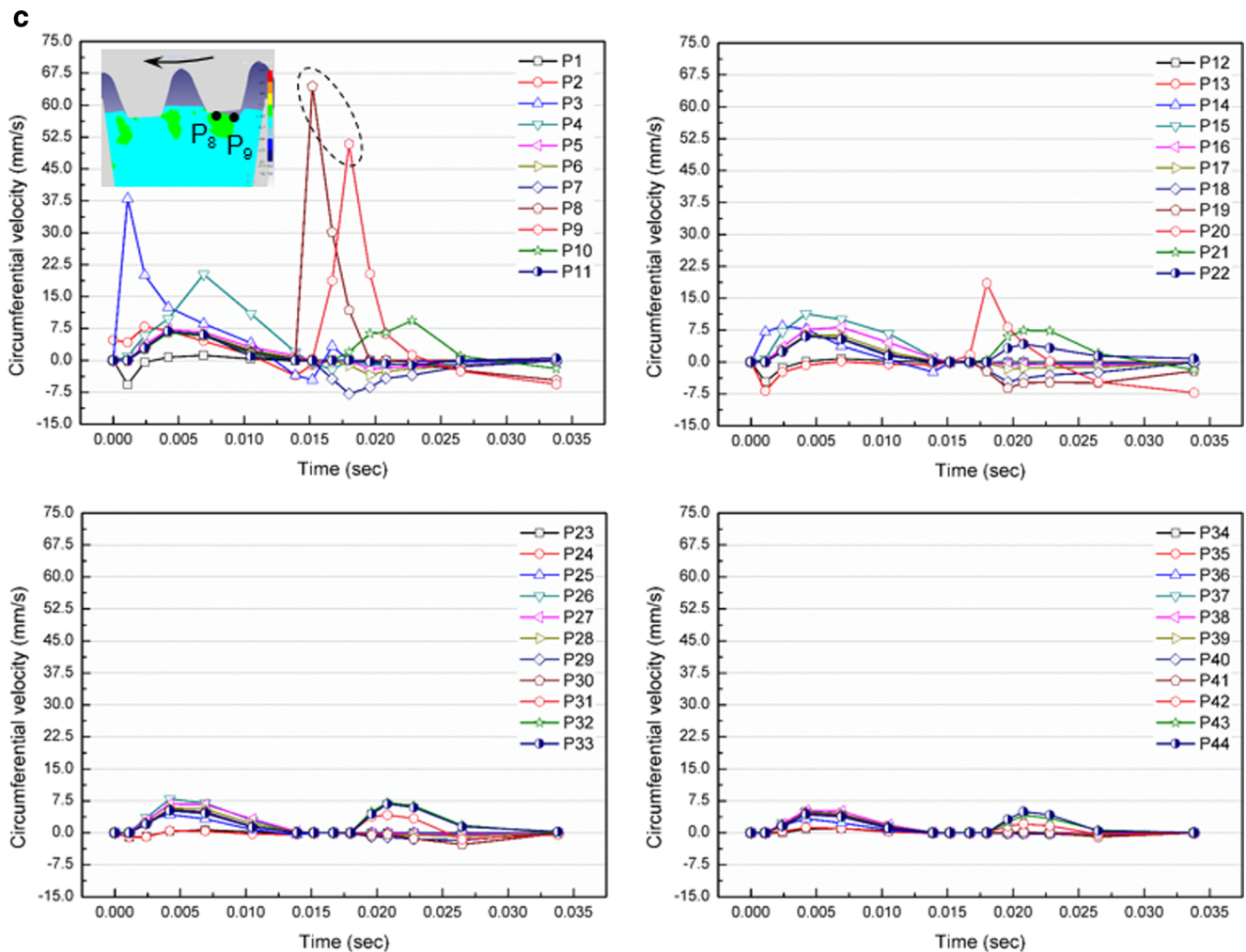


Fig. 9 (continued)

differences among velocity values of material particles on the two planes. The reason for this variation is believed to be the different tool penetration depths into the workpiece in the given time period. Furthermore, the points having maximum circumferential velocity are located near the root of the formed workpiece rather than on the flanks in the given time period. The reason for this trend can be explained by the form geometry of the rolling tools used in this investigation.

Circumferential displacement Figure 10 illustrates the displacements of material particles on planes III, IV, and V in the circumferential direction. As can be seen from Fig. 10 a, the circumferential displacements of material particles decrease with the increase of depths. The values of displacement of some material particles are always positive and negative during the rolling process, but those of other points are variable due to their position change. It can be observed from Fig. 10 b and c that the circumferential displacements of the

material particles on planes III and V are very similar and the displacement values decrease as the depth increases.

By observing Fig. 10 a–c, it can be found that the circumferential displacements of most material particles are positive during the rolling process, which indicates that the circumferential material flow is asymmetrical with respect to the symmetric line of the gear teeth to cause asymmetrical flanks of the formed gear, and that both positive and negative circumferential displacement maxima of the material particle on the plane IV are larger than those of planes III and V. This is because plane IV coincides with the mid-plane of the workpiece where the material is difficult to flow in the axial direction, and the material of planes III and V mainly flows in the axial direction.

4 Experiment

Although an experimental grid pattern (GP) cannot display characteristics such as the actual rolling stresses, strains,

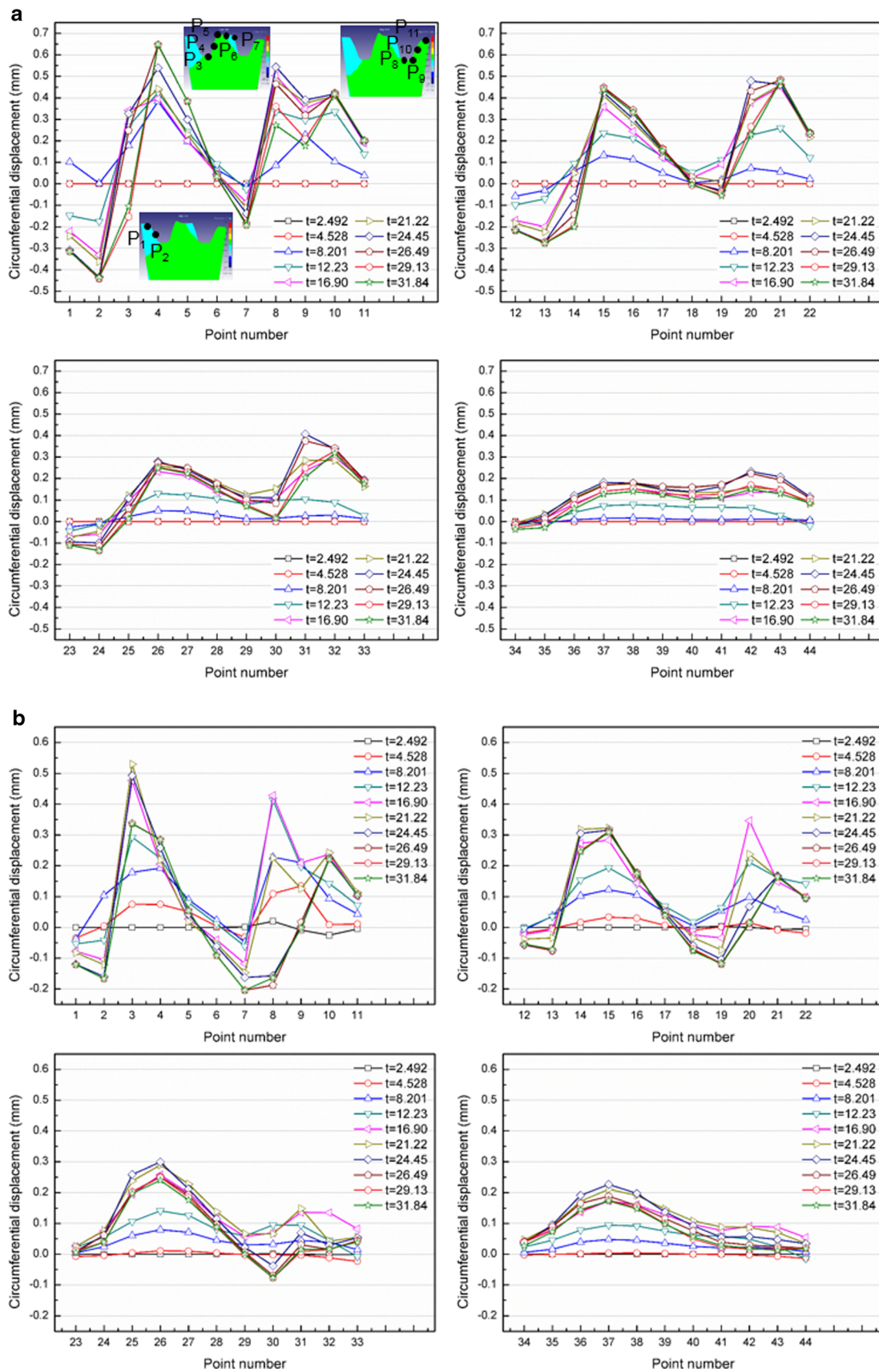


Fig. 10 Circumferential displacements of points on different planes. **a** Circumferential displacements of points on plane IV. **b** Circumferential displacements of points on plane III. **c** Circumferential displacements of points on plane V

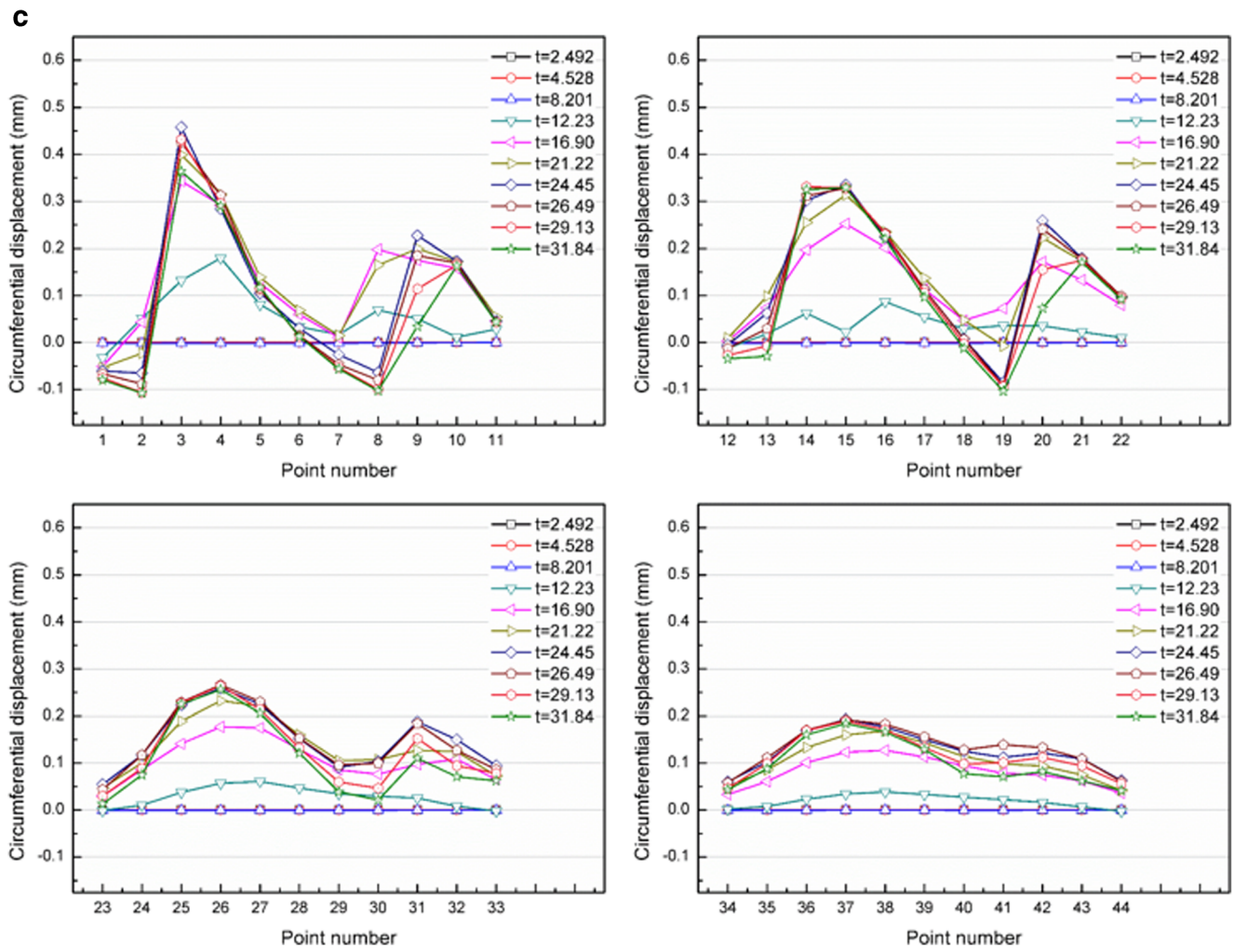


Fig. 10 (continued)

and temperature in real time, grid patterns can be used to visualize the material displacement field where metal flow is occurring. Grid patterns are also commonly used to check velocity fields but are assumed to be theoretical

results similar to FEA. However, the experimental GP method to record metal flow has been important for the visual understanding of the metal flow in an industrial process [31, 32].

Fig. 11 Experimental samples. a Sample dimensions. b Actual manufactured sample

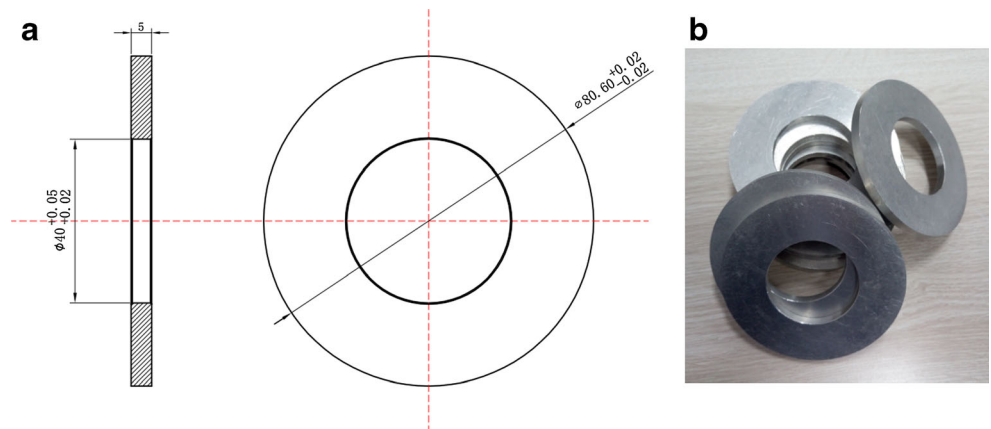


Fig. 12 Samples with grid patterns

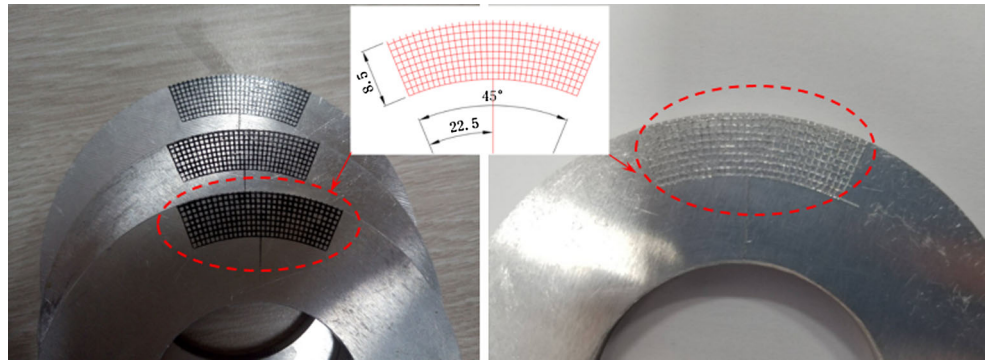


Fig. 13 The roll forming apparatus and forming defects

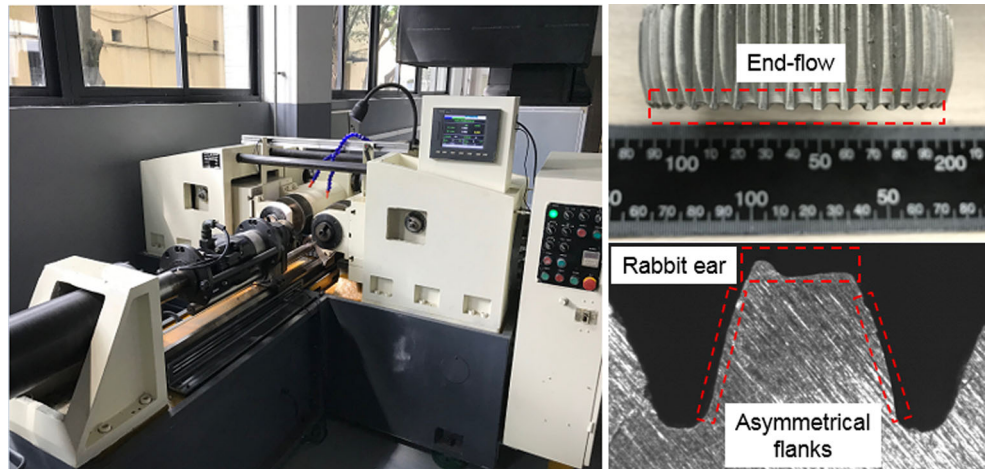
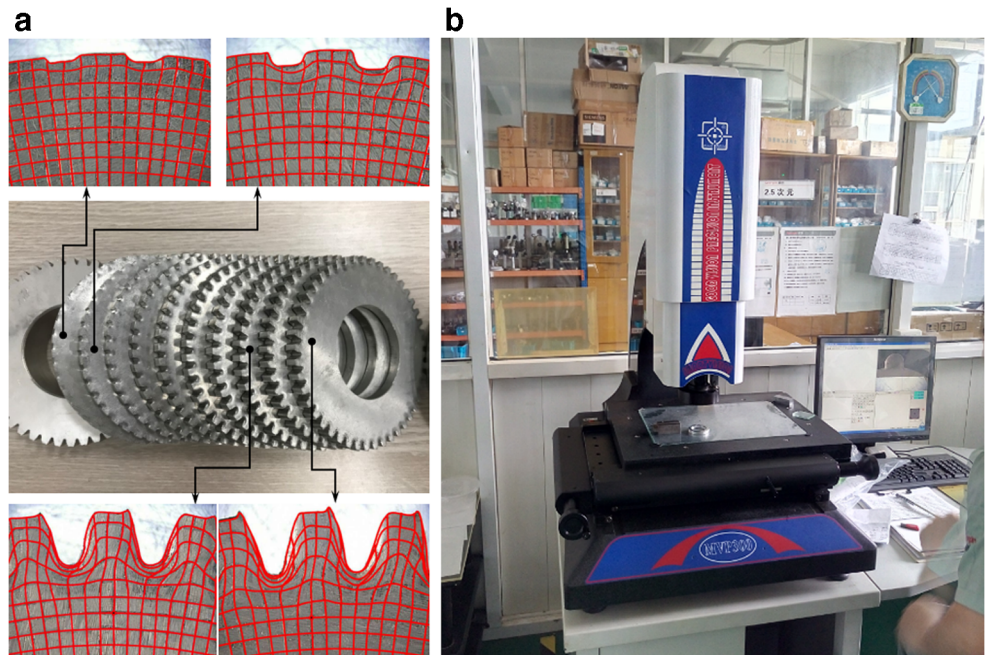


Fig. 14 The rolled samples and measuring system. a Grid appearance of the rolled sample. b Measuring system



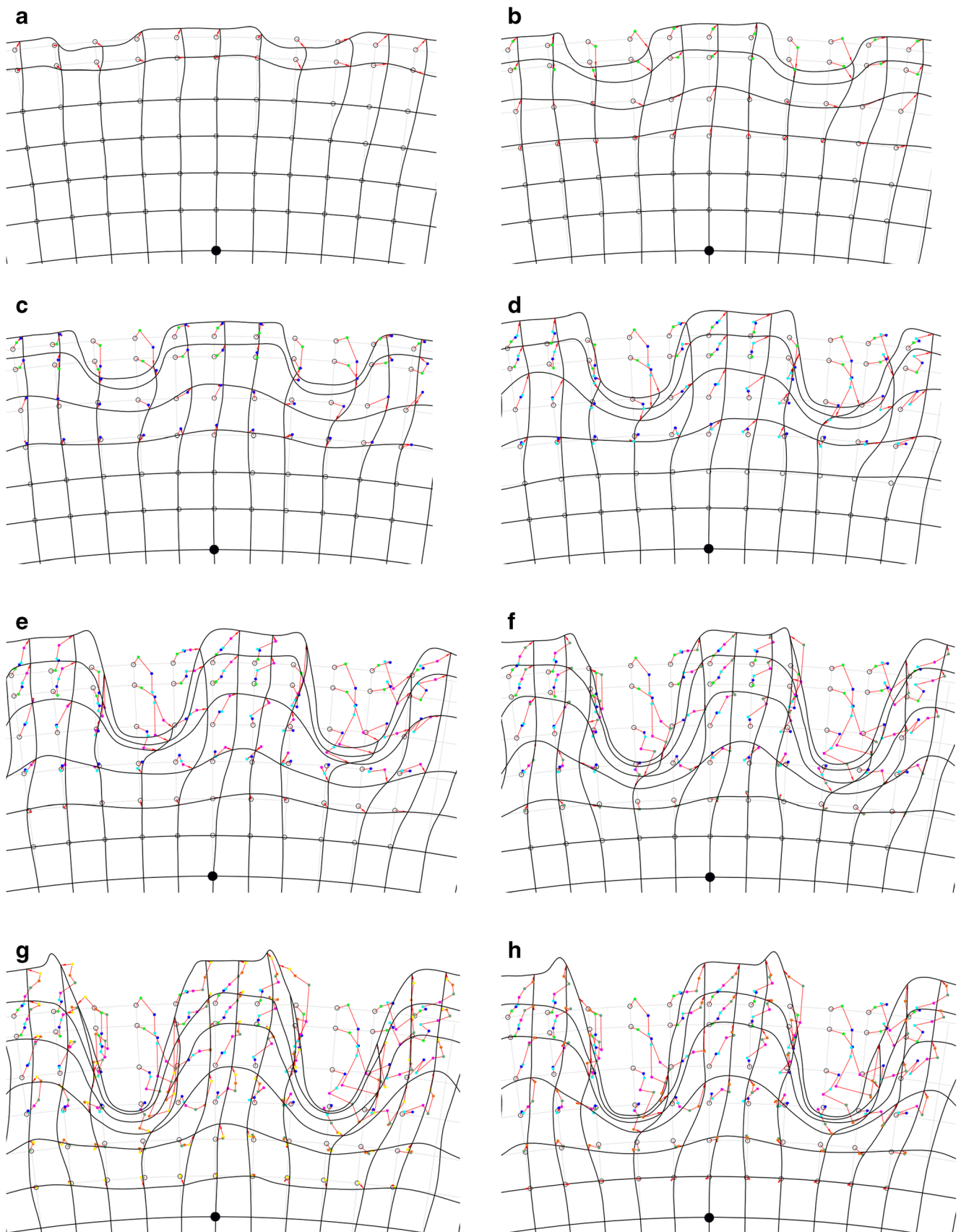


Fig. 15 The flow path of material. **a** 8% tool penetration. **b** 24% tool penetration. **c** 40% tool penetration. **(d)** 56% tool penetration. **e** 68% tool penetration. **(f)** 88% tool penetration. **g** 100% tool penetration. **(h)** 100% tool penetration

4.1 Experimental preparation

4.1.1 Samples

Metal plastic deformation can generally be assumed as a plane strain when the ratio of the tooth width to the tooth depth is larger than 4.5 [33]. To better understand the metal flow behavior inside of a workpiece subjected to roll forming, the slice method was employed in this section. The experimental sample thickness was 5 mm similar to the simulated thickness in the FEA discussed in Section 3.2. The ends of the samples were first ground to prepare the surface for gridding. The sizes of the samples can be seen in Fig. 11 a, and Fig. 11 b shows the actual manufactured samples.

The ink printing method was first used to layout the grids accurately on the face of the samples. Then, a single-tip stylus-embossing tool was utilized to permanently engrave over the ink grids into the sample material. Finally, the ink grids were cleaned away by a washing liquid, as shown in Fig. 12.

4.1.2 Experimental setup and parameter settings

Having simulated the metal flow during the gear throughfeed rolling process by FEA, corresponding experimental verification was conducted using the roll forming apparatus designed by authors, as shown in Fig. 13. All the experimental parameters were set the same as in the FEA simulation except the difference between the oil lubrication condition used in the experiment and friction coefficient set in FEA.

4.2 Measuring experimental data

The rolled samples shown in Fig. 14 a were photographed along their axial end planes to reveal the appearance of the final deformed grid patterns. An MVP Fully Automatic Video Measuring Machine produced by Good Vision Precision Instrument Co., Ltd., as shown in Fig. 14 b, was used to inspect the samples. The obtained photos were imported into AutoCAD®, and then their grids were highlighted by red lines. Finally, the node coordinates of the grids were measured and recorded.

4.3 Experimental result analysis

To illustrate the flow path of material in the gear throughfeed rolling process, the node coordinates were obtained from the recorded GP data and used to track material movement at different tool penetration depths into the workpiece. Different color points indicate the positions of material particles at different depths of tool penetration, and the length of the lines represents the flow displacements, as shown in Fig.

15. The flow progression of material particles and the tooth profile development can be divided into two roll forming stages depending on the depth of tool penetration: forming stage and finishing stage.

In the beginning of the forming stage, the material particles are mostly undeformed due to a small amount of tool penetration, and the deformation is situated on the contact zone between the workpiece and the teeth of rolling tool. As the teeth of rolling tools penetrate the workpiece surface, the material is continuously pushed to the bottom and to both sides of the tooth profile, as seen in Fig. 15 a. With continued tool penetration, the flow pattern of material is maintained along the radial and circumferential direction of the formed workpiece. Eventually, additional material is deformed as the tool penetration depth into the workpiece increases, as depicted in Fig. 15 b–g. The contact between the teeth of the rolling tool and both sides of the formed tooth profile is progressively unbalanced due to the direction of rolling and causes the circumferential displacement of material particles on the individually formed teeth to become unsymmetrical. Moreover, due to the difference of the flow velocities and directions between the surface and interior of each formed tooth, the development of the rabbit ear defect at each tooth crest is evident. It can be observed that the flow displacements of material particles in the radial direction are larger than those in the circumferential direction.

When the tool penetration nears 100%, this marks the end of the forming stage and the beginning of the finishing stage characterized by a comparatively small amount of metal deformation. If the tooth space of the rolling tool is small, the stress to obtain complete fill (100% tool penetration) is very high and can lead to tool breakage. Therefore, the radial flow of material is not restricted by the rolling tool at 100% tool penetration. This means that the material flow is still allowed, but the actual flow displacement which occurs is very small, as shown in Fig. 15 h. Additionally, the fact that roll forming is a local deformation process is evident due to the dead metal zone that exists in the interior of each tooth.

5 Conclusions

In this study, the three-dimensional material flow in gear profile formed by the forced throughfeed rolling process is analyzed. From the numerical and experimental analysis, the following conclusions are drawn:

- a. The material near the neutral plane hardly flows in the axial directions during the gear throughfeed rolling process. The average axial displacement at the formed crest of the workpiece ends amounts to approximately 15.4% of the displacement at the roots, and therefore, the end-flow originates in the roots of the workpiece ends.

- b. The material radial velocities of points on plane IV, plane III, and plane V are similar but not exactly the same. Compared to the radial displacement at the tooth crest on plane IV, it is reduced by 47.3% and 64.5% at the tooth crests on plane III and plane V, respectively. Moreover, the radial displacement differences of material at the tooth crests result in the rabbit ear formation due to the velocity gradient of material particles at the formed crests.
- c. The maximum circumferential velocity of material is located at the root of the formed workpiece due to the geometry of the rolling tools. Therefore, the geometry of rolling tools is a key factor that affects material flow in the gear forced throughfeed rolling process.
- d. When the teeth of the rolling tools sequentially contact both sides of the tooth profile in single-direction rolling, the circumferential flow displacements of material on the individual formed tooth are asymmetrical, and this results in the defect of asymmetrical flanks. Moreover, the flow displacements of material in the radial direction are larger than those in the circumferential direction.
- e. An understanding of material flow in the forming process leads to the foundation on reducing the defects and improving the quality of the formed gear in future work.

Acknowledgments The authors extend sincere gratitude to Yawen Wang, Department of Mechanical and Aerospace Engineering, University of Texas at Arlington, Arlington, Texas, USA, for his editing and technical advice.

Funding information This study was funded by the National Natural Science Foundation of China (Grant No. 51775062) and the Research Project of State Key Laboratory of Mechanical Transmission (Grant No. SKLMT-ZZKT-2015T01).

References

1. Kamounh AA, Ni J, Stephenson D, Vriesen R, DeGrace G (2007) Diagnosis of involutometric issues in flat rolling of external helical gears through the use of finite-element models. *Int J Mach Tools Manuf* 47:1257–1262. <https://doi.org/10.1016/j.ijmachtools.2006.08.015>
2. Kamounh AA, Ni J, Stephenson D, Vriesen R (2007) Investigation of work hardening of flat-rolled helical-involute gears through grain-flow analysis, FE-modeling, and strain signature. *Int J Mach Tools Manuf* 47:1285–1291. <https://doi.org/10.1016/j.ijmachtools.2006.08.015>
3. Neugebauer R, Putz M, Hellfritsch U (2007) Improved process design and quality for gear manufacturing with flat and round rolling. *Ann CIRP* 56(1):307–312. <https://doi.org/10.1016/j.cirp.2007.05.071>
4. Neugebauer R, Klug D, Hellfritsch U (2007) Description of the interaction during gear rolling as a basis for a method for the prognosis of the attainable quality parameters. *Prod Eng* 1(3):253–257. <https://doi.org/10.1007/s11740-007-0041-9>
5. Neugebauer R, Hellfritsch U, Lahl M (2008) Advanced process limits by rolling of helical gears. *Int J Mater Form* 1(1):1183–1186. <https://doi.org/10.1007/s12289-008-0152-7>
6. Khodae A, Melander A (2014) A study of the effects of reversal cycle in the gear rolling process by using finite element simulations. *Key Eng Mater* 611-612(3):134–141. <https://doi.org/10.4028/www.scientific.net/kem.611-612.134>
7. Kretzschmar J, Stockmann M, Lhlemann J, Schiller S, Hellfritsch U (2015) Experimental–numerical investigation of the rolling process of high gears. *Exp Tech* 39:28–36. <https://doi.org/10.1111/ext.12016>
8. Li J, Wang GC, Wu T (2016) Numerical simulation and experimental study of slippage in gear rolling. *J Mater Process Technol* 234: 280–289. <https://doi.org/10.1016/j.jmatprotec.2016.03.030>
9. Li J, Wang GC, Wu T (2017) Numerical-experimental investigation on the rabbit ear formation mechanism in gear rolling. *Int J Adv Manuf Technol* 91(9–12):3551–3559. <https://doi.org/10.1007/s00170-017-0009-7>
10. Ma ZY, Luo YX, Wang YQ (2018) On the pitch error in the initial stage of gear roll-forming with axial-infeed. *J Mater Process Technol* 252:659–672. <https://doi.org/10.1016/j.jmatprotec.2017.10.023>
11. Ma ZY, Luo YX, Wang YQ (2017) Study on the pitch error in the initial stage of gear rolling process. *ASME Int Power Trans Gear Conf* 10
12. Zhu XX, Zhu Y, Wang SS, Wang BY (2015) Numerical simulation and experiment of hot roll forming large module spur gear. *Mach Des Manuf-Chin* 7:67–69. <https://doi.org/10.3969/j.issn.1001-3997.2015.07.020>
13. Domblesky JP, Feng F (2002) A parametric study of process parameters in external thread rolling. *J Mater Process Technol* 121: 341–349. [https://doi.org/10.1016/S0924-0136\(01\)01223-7](https://doi.org/10.1016/S0924-0136(01)01223-7)
14. Siczekarek P, Wernicke S, Gies S, Martins PAF, Tekkaya AE (2016) Incipient and repeatable plastic flow in incremental sheet-bulk forming of gears. *Int J Adv Manuf Technol* 86:3091–3100. <https://doi.org/10.1007/s00170-016-8442-6>
15. Yan HJ, Wang LJ, Liu YZ, Li GC, Liu JP, Hu ZH (2014) Effect of thread helix angle on the axial metal flow of cross wedge rolling thread shaft. *Appl Mech Mater* 440:177–181. <https://doi.org/10.4028/www.scientific.net/AMM.440.177>
16. Cui FK, Wang XQ, Zhang FS, Xu HY, Quan JH, Li Y (2013) Metal flowing of involute spline cold roll-beating forming. *Chin J Mech Eng* 26(5):1056–1062. <https://doi.org/10.3901/CJME.2013.05.1056>
17. Liu ZQ, Song JL, Qi HP, Li YT, Li XD (2010) Parameters and experiments on the precision forming process of spline cold rolling. *Appl Mech Mater* 34-35:646–650. <https://doi.org/10.4028/www.scientific.net/AMM.34-35.646>
18. Pater Z, Gontarz A, Weroński W (2004) New method of thread rolling. *J Mater Process Technol* 153-154:722–728. <https://doi.org/10.1016/j.jmatprotec.2004.04.154>
19. Szota PL, Dyja H (2006) Numerical modeling of the metal flow during the rolling process of the round screw-ribbed bar in the finishing pass. *J Mater Process Technol* 177:566–569. <https://doi.org/10.1016/j.jmatprotec.2006.04.035>
20. Groche P, Kramer P (2017) Numerical investigation of the influence of frictional conditions in thread rolling operations with flat dies. *Int J Mater Form* 3:1–17. <https://doi.org/10.1007/s12289-017-1383-2>
21. Zhang DW, Zhao SD (2014) New method for forming shaft having thread and spline by rolling with round dies. *Int J Adv Manuf Technol* 70:1455–1462. <https://doi.org/10.1007/s00170-013-5387-x>
22. Cui MC, Zhao SD, Zhang DW, Chen C, Li YY (2017) Finite element analysis on axial-pushed incremental warm rolling process of spline shaft with 42CrMo steel and relevant improvement. *Int J Adv Manuf Technol* 90:2477–2490. <https://doi.org/10.1007/s00170-016-9566-4>

23. Ma ZY, Luo YX, Wang YQ, Wang Y (2018) Integrity and modeling of gear tooth forming in the roll-forming of gear with axial infeed. *J Mech Eng-Chin* 54(6):133–145. <https://doi.org/10.3901/JME.2018.06.133>
24. Ma ZY, Luo YX, Wang YQ, Mao J (2018) Geometric design of the rolling tool for gear roll-forming process with axial infeed. *J Mater Process Technol* 258:67–79. <https://doi.org/10.1016/j.jmatprotec.2018.03.006>
25. Neugebauer R, Hellfritzsich U, Lahl M, Schiller S, Milbrandt M (2011) Innovations in rolling process of helical gears. *AIP Conf Proc* 1315:569–574. <https://doi.org/10.1063/1.3552507>
26. Khodae A (2015) Gear rolling for production of high gears. Dissertation, KTH Royal Institute of Technology
27. Li F, Lin JF, Chu GN (2009) Metal flow in the precision forging of aluminum alloys. *JOM* 61(8):57–60
28. Valberg H (2010) Comparison of metal flow in un-lubricated direct and indirect extrusion of aluminum alloys. *Int J Mater Form* 3:387–390. <https://doi.org/10.1007/s12289-010-0788-y>
29. Shen XH, Chen W, Yan J, Zhang L, Zhang J (2015) Experiment and simulation of metal flow in multi-stage forming process of railway wheel. *J Iron Steel Res, Int* 22(1):21–29. [https://doi.org/10.1016/S1006-706X\(15\)60004-8](https://doi.org/10.1016/S1006-706X(15)60004-8)
30. Yang MS, Yuan QL, Li Y, Zheng JM (2011) Deformation force simulation of lead screw cold roll-beating. *Prod Eng* 15:5164–5169. <https://doi.org/10.1016/j.proeng.2011.08.958>
31. Valberg H (2012) Characterization of metal flow in metals processing by a combined approach using advanced experimental grid pattern techniques coupled with FE-analysis. *ICAA13* 1501–1513. https://doi.org/10.1007/978-3-319-48761-8_227
32. Li F, Lin JF, Yuan SJ, Liu XJ (2009) Effect of inner cone punch on metal flow in extrusion process. *Int J Adv Manuf Technol* 42:489–496. <https://doi.org/10.1007/s00170-008-1806-9>
33. Wang ZK, Zhang Q (2008) Numerical simulation of involutes spline shaft in cold rolling forming. *J Cent South Univ Technol* 15(s2):278–283. <https://doi.org/10.1007/s11771-008-0471-3>

Publisher's note Springer Nature remains neutral with regard to jurisdictional claims in published maps and institutional affiliations.